Finite Element Analysis of the Parameters Influencing the Failure Modes of Carbon Fiber Reinforced Polymer Cores

JIAYUN CAO[1], XIAOMIN ZHANG[2], HONGBO CHEN[3], AND YU JIANG[1]

[1]College of Materials Science and Engineering, Sichuan University, Chengdu 610065, China
[2]Sichuan Shuneng Electric Power Company Ltd., Gaoxin District Branch, Chengdu 610065, China
[3]State Grid Sichuan Electric Power Research Institute, Chengdu 610065, China

Corresponding author: Yu Jiang (jyscuniversity@163.com)

ABSTRACT Carbon fiber reinforced polymer (CFRP) is an anisotropic material with outstanding tensile strength in the axial direction but low compressive strength in the radial direction. In the process of line construction, such as wire crimping and conductor clamping, radial pressure failure and slip failure easily occur. This paper applies finite element analysis (FEA) to the parameters influencing the radial stress and displacement in a CFRP core to research the failure modes of the CFRP core. The selected parameters are the interference of the CFRP core, the friction coefficient between the core and inner wedge, and the angle of the inner wedge. The finite element method is applied to analyze a CFRP core with a self-tightening clamp to find the optimum condition parameters so that the CFRP core experiences neither slip failure nor radial pressure failure. From the study, lower interference and larger friction coefficient and angle lead to lower radial stress. The interference has the largest effect on the mitigation of radial pressure failure. For larger interference, a larger friction coefficient and angle mitigate slip failure. According to the analytic results, an interference between 0.02 mm and 0.025 mm and an angle larger than 3°, coupled with a friction coefficient larger than 0.3, best stop slip failure and radial pressure failure.

INDEX TERMS CFRP core, finite element analysis, radial pressure failure, slip failure, self-tightening clamp.

I. INTRODUCTION

As carriers of electric power, overhead conductors play an important role in transmission lines [1]–[3]. The overhead conductors currently used consist of aluminum strands wrapped around a steel core, where the aluminum strands carry the current and the steel core supports the mechanical load [4]. With the rapid development of society, the electrical load has increased rapidly [5], [6]. Traditional aluminum conductor steel reinforced (ACSR) transmission lines no longer meet the increasing power load demands [7]. To increase the grid capacity, new conductors with large carrying capacity have been introduced. One such class of conductors is high-voltage, carbon fiber composite core conductors, in which the steel core used in conventional conductors is replaced with a composite core [8]–[10]. The composite core comprises continuous carbon and glass fibers in an epoxy matrix,

carbon composite in the center, and a glass composite shell around it. For the convenience of analysis, the carbon fiber and glass fiber are treated as a carbon fiber reinforced polymer (CFRP) core. Compared to the traditional aluminum conductors with steel cores, the composite core conditions have higher tensile strength, higher operating temperature, higher specific strength, lighter weight, and better corrosion resistance [11]–[14].

Ahmad Alawar *et al.* [15] state that conventional steel cable conductors were replaced with a composite core conductor with high strength. Shuai Du *et al.* [16] studied the corrosion resistance and heat resistance of carbon fiber composite core conductors and traditional steel core aluminum conductors, and the results showed that the corrosion resistance and heat resistance of the carbon fiber composite core conductors were better than those of the traditional steel core aluminum conductors. Meenakshi S *et al.* [17] investigated the influences of different types and thicknesses of composite materials and different angles of lamination on the properties

The associate editor coordinating the review of this manuscript and approving it for publication was Guijun Li.

of lightweight thermoplastic composites by using numerical analysis. Sathiyamoorthy Margabandu *et al.* [18] experimentally studied the effects of different layering methods on the bending and impact properties of laminated jute/carbon hybrid composites in an epoxy matrix, and the experimental results were validated numerically. Research by Brunair RM and Cardou A [19], [20] showed that failures of conventional overhead conductors generally occur at the location where the conductor is attached to the lattice tower. N.K. Kar *et al.* [21] reported that fatigue of composite rods and slip failure and compressive crushing of composite rods are associated with this process. Jong Sup Park *et al.* [22] examined the parameters influencing the shear stress and displacement of CFRP tendons through finite element analysis (FEA). Unlike conventional steel cores, CFRP is an anisotropic material [23]–[26]. It has superior strength characteristics in the direction of the fibers but inferior lateral strength in the direction perpendicular to the fibers [27], placing limitations on the immediate use of the overhead conductor.

This paper presents a study on the slip failure and radial pressure failure characteristics of a CFRP core with a self-tightening strain clamp in order to manufacture the optimal self-tightening clamp. For that goal, a FEA study was carried out to understand the effect of radial pressure failure and slip failure on different parameters in this study. The impacts of the interference, friction coefficient, and angle were investigated through a parametric study to determine the optimal combination of parameters. Thereby, the carbon fiber composite core conductor and self-tightening clamp can be further developed and be more widely applied. Finally, the simulation results were validated experimentally.

II. ANALYSIS OF THE FAILURE MODES

High-voltage transmission lines are suspended between lattice towers by tensioning, and consequently, the CFRP cores in these lines experience static axial tensile stress [21]. Therefore, the core moves in the axial direction. Additionally, the initial interference causes a radial clamping force, so the core moves outward together with the inner wedge. In addition, using the self-tightening principle, the wedge holder reacts to the inner wedge, so with the outward core movement, the inner wedge is hampered by the wedge holder. Figure 1 shows the design of a self-tightening fixture used to grip the CFRP core and the forces acting due to tensile load. There is a confining force between the core and the inner wedge from the self-tightening clamp. This confining force is a friction force that occurs in the direction parallel to the contact surface and varies with respect to the radial clamping force and friction coefficient.

The failure modes are shown in Figure 2. Slip failure may occur because of a decrease in the radial force necessary for the self-tightening clamp due to interference. However, radial pressure failure may occur due to an increase in the radial clamping force of the CFRP core.
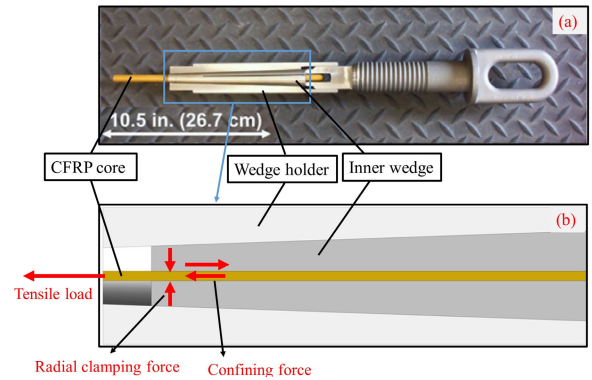

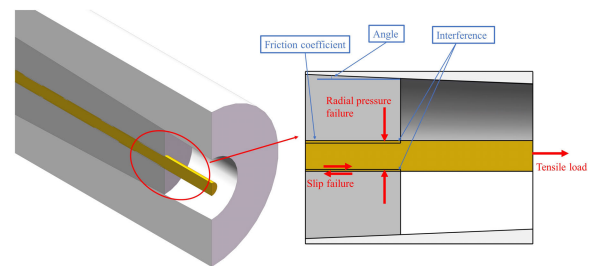**FIGURE 1.** Self-tightening strain clamp and acting forces.

FIGURE 2. Failure modes and main influential factors.

TABLE 1. Mechanical properties of CFRP core.

Young's Modulus/GPa			Poisson's Ratio			Shear Modulus/GPa		
X	Y	Z	XY	YZ	XZ	XY	YZ	XZ
209	94.5	94.5	0.27	0.4	0.27	55	39	55

Accordingly, the factors significantly influencing the radial clamping force generated by the wedge action need to be examined to ensure the appropriate confining force from the self-tightening strain clamp. The major factors affecting the failure mechanism of the self-tightening strain clamp are the friction coefficient between the CFRP core and the inner wedge and the interference between the core and the inner wedge. The key influential factors are shown in Figure 2.

III. FINITE ELEMENT MODEL

The model considered in the analysis is composed of the CFRP core, the inner wedge, and the wedge holder (Figure 1). Its exact dimensions are shown in Figure 3, and the inner angle varies depending upon the simulation requirements. According to the geometric size, a three-dimensional model of the specimen is created with SolidWorks.

The wedge holder and the inner wedge are assumed to be made of 1Cr18Ni9 austenitic stainless steel with an elastic modulus of 200 GPa and a Poisson's ratio of 0.3. The CFRP core has a nominal diameter of 6 mm; this value is used in the analysis, which is considered to be anisotropic, and the mechanical properties are listed in Table 1.
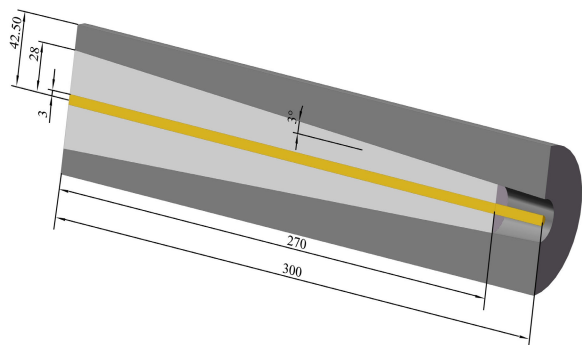
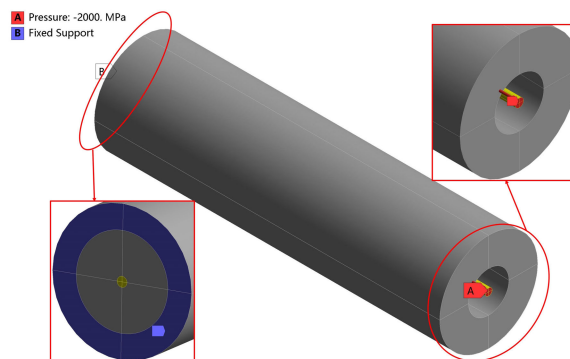FIGURE 3. Exact dimensions of self-tightening strain clamp.
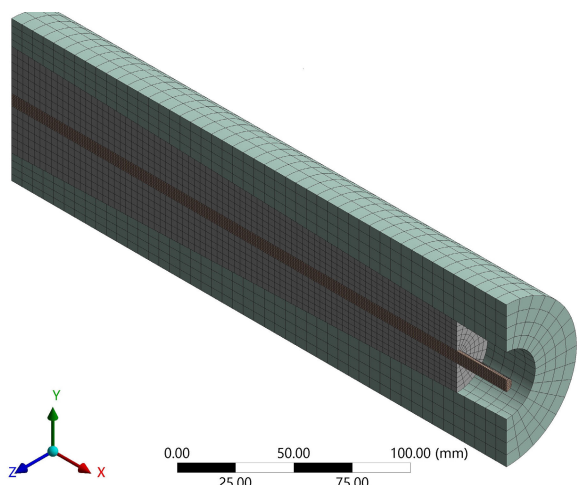

FIGURE 5. Load and Boundary conditions.

FIGURE 4. Finite element model of CFRP core and strain clamp.

The model is meshed using SOLID186 3D 20 node structural elements to obtain an accurate analysis. This type of element is suitable for modeling curved boundaries and can tolerate irregular shapes without much loss of accuracy. The meshing at the CFRP core is finer for more accurate results, and that at the inner wedge and the wedge holder is thicker to reduce the computation time. Figure 4 shows the half meshed model. There are 31,776 elements and 172,580 nodes in the finite element model.

Face-to-face contact between the CFRP core and strain clamp is used to model the interaction of the different parts. There are two contact pairs when setting up surface contact. In the first pair, since the outer surface of the core is convex, the inner surface of the inner wedge is concave. According to the selection principle of the contact surface and target surface [28]–[31], the convex surface is the contact surface, and the concave surface is the target surface. According to engineering analysis, the CFRP core is the research object and should be set as the contact surface. Therefore, according to the above description, the outer surface of the core should be defined as the contact surface, and the inner surface of the inner wedge should be defined as the target surface. The contact method is frictional contact. The CFRP core and

inner wedge and the inner wedge and wedge holder are both fully fitted in geometric modeling, but in practical applications, there is interference between the core and the inner wedge. The friction coefficient and interference are adopted as parameters in the analysis. The friction coefficient is varied from 0.1 to 0.4 assuming smooth to coarse. In the second pair, the outer surface of the inner wedge is chosen as the contact surface, and the inner surface of the wedge holder is chosen as the target surface. The contact type is no separation contact, and the rest is set to the default. The friction force occurring in the direction parallel to the contact surface varies with the size of the input coefficient of friction.

As can be seen from the structure of the self-tightening strain clamp in Figure 1(a), the bottom of the wedge holder (opposite the loaded face) fixed by a nut. Therefore, in the simulation, in order to be consistent with the actual working conditions, the bottom of the wedge holder should also be fixed. In the Figure 5, the bottom of the self-tightening clamp is enlarged and displayed. You can see that the bottom of the wedge holder is blue, indicating that it has been set as a fixed constraint.

The tensile strength of the CFRP core is 2231MPa. In order to facilitate calculation and assume the ultimate load of the CFRP, an integer load of 2000MPa corresponding to the tensile strength is taken to act on the CFRP core to evaluate the behavior of the failure of the core. In the Figure 5, the top of the self-tightening clamp is enlarged and displayed. You can see that the top of the CFRP core is red, indicating that it has been set as load condition.

To prevent rigid body motion, the option 'weak spring' and 'large deflection' is turned on. Finally, static analysis simulations are carried out to obtain the displacement and radial stress results with the Lagrangian approach to reduce the computational time.

IV. FAILURE CRITERION FOR CFRP CORE
The CFRP core is an anisotropic material, and its strength varies in different principal directions, so the traditional von Mises criterion cannot be used to estimate the failure of the CFRP core. The maximum stress criterion of the composite material strength criterion is adopted in this study [32].

TABLE 2. Ultimate strength of CFRP core in all directions.

	Tensile strength/MPa			Compressive strength/MPa			Shear strengths/MPa	
X	Y	Z	X	Y	Z	XY	YZ	XZ
2231	29	29	1082	100	100	60	32	60

As long as any stress component in the principal direction of the CFRP core reaches the corresponding ultimate strength, the CFRP core fails.

For the tensile stress: $\sigma > 0$

$$\left.\begin{array}{c} \sigma_1 < X_t \\ \sigma_2 < Y_t \end{array}\right\} \quad (1)$$

For the compressive stress: $\sigma < 0$

$$\left.\begin{array}{c} |\sigma_1| < X_c \\ |\sigma_2| < Y_c \end{array}\right\} \quad (2)$$

where σ_1, σ_2 are two stress components along the principal direction of the material (σ_1 is the stress along with the fiber, σ_2 is the stress vertical the fiber). X_t, Y_t are tensile strength along the fiber direction and perpendicular to the fiber direction. X_c, Y_c are compressive strength along the fiber direction and perpendicular to the fiber direction.

As shown in Figure 4, the axial direction is along the fiber direction and is the X-direction in the coordinate system. The radial direction is vertical to the fiber direction and is the Y-direction in the coordinate system. The ultimate strength of the CFRP core in all directions is shown in Table 2, and its radial compressive strength is 100 MPa. Because its radial compressive strength is low and it is prone to radial compressive failure in actual working conditions, when considering strength failure, the main consideration is radial compressive failure. The radial stress and the radial compressive strength of the simulated CFRP core under different parameters are compared. If the absolute value of the radial stress suffered by the CFRP core is greater than 100 MPa, then the core is judged to experience compressive failure; otherwise, the CFRP core experiences no compressive failure. (In this paper, all the radial stresses and compressive strengths are turned into absolute values. To avoid repetition, this is not described in this paper.)

In this simulation, if the tensile load of the core is greater than the friction force of the core, the core undergoes axial displacement due to unbalanced forces. There is no numerical solution in FEA when encountering unbalanced forces. Therefore, when this simulation does not have the numerical solution, the CFRP core slip fails; otherwise, no slip failure occurs.

V. RESULTS AND DISCUSSION

The analysis consists of two phases. The first phase of analysis finds the range of parameters leading to no slip failure. The second phase of analysis is performed to understand the effect of each parameter on the failure modes of the CFRP core.

TABLE 3. Radial stress and displacement per parameter.

Interference/mm	Friction coefficient	Angle/°	Radial stress/MPa	Displacement/mm
0.0175	0.1	4	—	—
0.0175	0.2	3	—	—
0.0175	0.3	2	—	—
0.0175	0.4	1	—	—
0.02	0.1	1	—	—
0.02	0.1	4	—	—
0.02	0.4	1	—	—
0.02	0.4	4	78.15	1.93
0.0225	0.2	2	94.11	3.05
0.0225	0.2	3	91.15	2.89
0.0225	0.3	2	91.86	2.32
0.0225	0.3	3	89.19	2.14
0.025	0.1	1	—	—
0.025	0.2	2	102.45	2.74
0.025	0.3	3	97.3	1.92
0.025	0.4	4	94.36	1.48
0.0275	0.2	2	110.98	2.49
0.0275	0.2	3	108.06	2.35
0.0275	0.3	2	108.92	1.96
0.0275	0.3	3	105.69	1.73
0.03	0.1	1	—	—
0.03	0.1	4	—	—
0.03	0.4	1	—	—
0.03	0.4	4	126.17	1.27

The first phase of analysis is based on interferences from 0.0175 mm to 0.03 mm, friction coefficients from 0.1 to 0.4 and angles from 1° to 4°. Estimated slip failure occurs regardless of whether there is a numerical solution under each set of parameters. If there is a numerical solution, no slip failure occurs for this set of parameters. If not, slip failure occurs.

The analysis is conducted for a total of 24 cases. The radial stress developed in the CFRP core and the displacement of the core at its loaded end are as follows. As listed in Table 3, of these 24 cases, 11 cases have no numerical solutions. In these 11 cases, the interference is 0.0175 mm, the friction coefficient is 0.1 or the angle is 1°. This means that slip failure occurs. Hence, to prevent slip failure, the interferences should be larger than 0.02 mm, the friction coefficient should be larger than 0.2, and the angle should be larger than 1°.

The second phase of the study analyzes the effect of each parameter on the failure modes of a CFRP core with a self-tightening strain clamp. This phase of the study considers interferences from 0.02 mm to 0.03 mm, friction coefficients from 0.2 to 0.4 and angles from 1° to 4°.

A. EFFECTS OF THE ANGLE AND FRICTION COEFFICIENT

Figure 6 plots the radial stress and displacement of the CFRP core with respect to the angle and friction coefficient in the case of identical interference. In this plot, the friction coefficient is between 0.2 and 0.4, and the angle is between 1° and 4°.

As shown in Figure 6, the radial stress decreases significantly for angles from 2° to 3.5°, but the radial stress increases slightly for angles from 3.5° to 4°. This means that the minimum radial stress occurs at an angle of 3.5°.
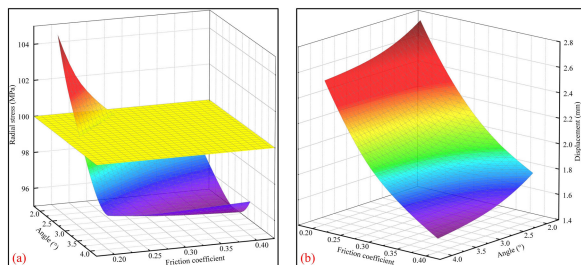
FIGURE 6. Radial stress and displacement with respect to angle and friction coefficient.(a) Radial stress; (b) Displacement.

FIGURE 7. Radial stress and displacement with respect to angle and interference.(a) Radial stress; (b) Displacement.

FIGURE 8. Radial stress and displacement with respect to interference and friction coefficient.(a) Radial stress; (b) Displacement.

The maximum radial stress for a friction coefficient of 0.2 and an angle of 2° reaches 104.69 MPa, which exceeds the radial compressive strength of the CFRP core. For a friction coefficient of 0.2 and an inner wedge with an angle of 3.5°, the minimum radial stress reaches 95.79 MPa, corresponding to a reduction of approximately 8.5% compared to the maximum radial stress. This is a small change in the radial stress. This shows that the angle and the friction coefficient have little effect on the radial stress compared to the interference.When the Angle is 3.5°, the minimum radial stress of the CFRP core is 95.79MPa, which does not exceed the compressive strength of the CFRP core of 100 MPa, and the radial pressure failure will not occur at this time. And when the angle is 3.5°, no matter how large the friction coefficient is, there is a numerical solution for the displacement of the CFRP core, and slip failure will not occur.

To prevent radial pressure failure, the radial stress of the CFRP core must be less than the compressive strength of the CFRP core of 100 MPa, so the angle should be larger than 3° and the friction coefficient should be larger than 0.3.

The displacement of the CFRP core decreases significantly with a larger friction coefficient and decreases slightly with a larger angle. The displacements for angles of 2° and 4° reach 2.77 mm and 2.53 mm, respectively, in the case of a friction coefficient of 0.2. The displacements for angles of 2° and 4° reach 1.77 mm and 1.51 mm, respectively, in the case of a friction coefficient of 0.4. There are differences of 8.6% and 14.7% between these two angles and differences of 36.1% and 40.3% between these two friction coefficients. This means that the friction coefficient affects the displacement more than the angle.

B. EFFECTS OF THE INTERFERENCE AND ANGLE

Figure 7 plots the radial stress and displacement of the core according to the interference and angle. In this plot, the angle is between 2° and 4°, and the interference is between 0.02 mm and 0.03 mm.

The radial stress in the CFRP core remarkably increases with larger interference.

As shown in Figure 7, the interference has a larger effect on the radial stress of the CFRP core than the angle. The radial stress occurring in the core with the interference varies from 83.89 MPa and 116.69 MPa in the case of an angle
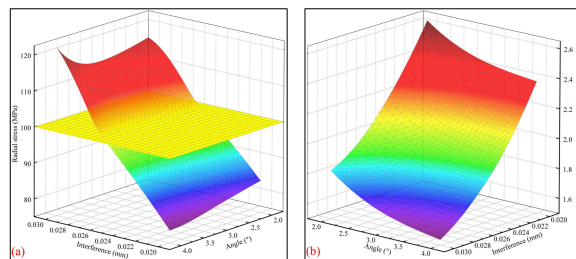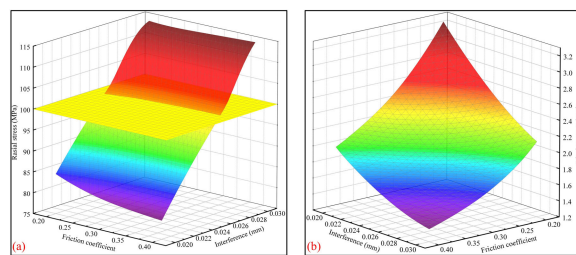
of 2°. The radial stress with the interference varies from 78.47 MPa and 121.7 MPa in the case of an angle of 4°. There are differences of 28.1% and 35.5% between the two interferences and differences of 6.4% and 4.2% between the two angles. Accordingly, the interference appears to be effective in reducing the radial stress occurring at the CFRP core. When the interference is assumed to be larger than 0.025 mm, the radial stress reaches 100 MPa, resulting in radial pressure failure of the CFRP core. To prevent radial pressure failure, the interference should be lower than 0.025 mm.

In Figure 7(b), the plot of the displacement of the CFRP core with respect to the angle and interference shows that there is a comparatively larger difference with the interference than with the angle of the displacement. Therefore, the slip of the CFRP core becomes significant with lower interference.

C. EFFECTS OF THE FRICTION COEFFICIENT AND INTERFERENCE

Figure 8 plots the radial stress with the friction coefficient and interference. In the plot, the friction coefficient is between 0.2 and 0.4, and the interference is between 0.02 mm and 0.03 mm.

The minimum radial stress developed in the CFRP core is 79.44 MPa when the interference is 0.02 and the friction coefficient is 0.4. In addition, the maximum radial stress is 114.77 MPa when the interference is 0.03 and the friction coefficient is 0.4. This shows that the radial stress increases significantly with larger interference. The radial stress with the friction coefficient remains almost invariable compared to that with the interference, which shows that the friction coefficient has little effect on the radial stress. However, when
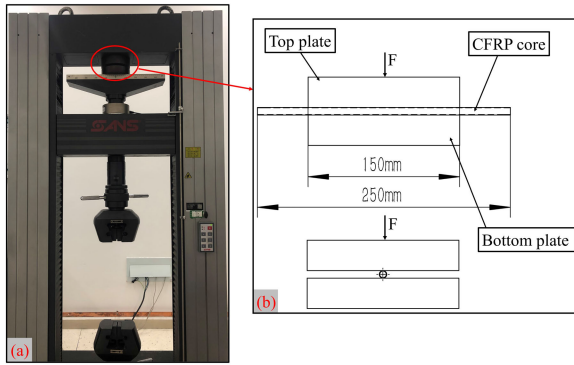
FIGURE 9. The UTM (a) and the principle of radial pressure test (b).

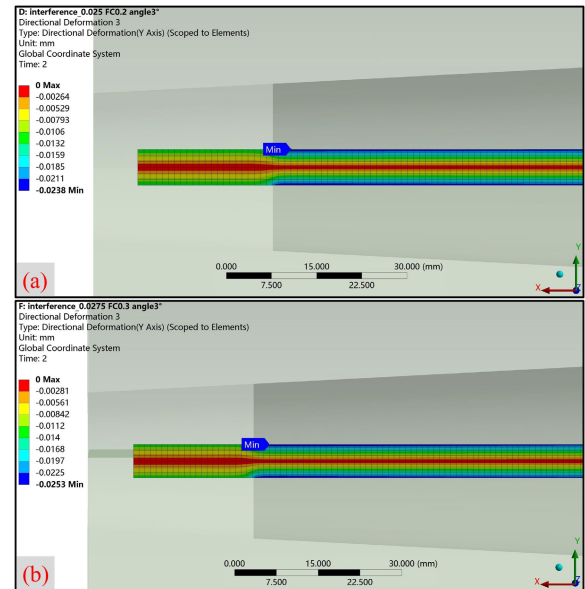**FIGURE 10.** Comparison of CFRP core test samples before and after test.

FIGURE 11. Y direction deformation of two numerical cases.

TABLE 4. Radial deformation of experimental and numerical(mm).

Experimental				Numerical	
1	2	3	4	1	2
0.045	0.041	0.05	0.043	0.048	0.05

the interference is small, the radial stress developed in the core appears to be smaller with larger friction coefficients.

The analysis reveals that when the interference is larger than 0.025 mm, the radial stress of the CFRP core exceeds a radial compressive strength of 100 MPa.

Unlike the radial stress, the displacement of the core decreases with a larger interference and friction coefficient. When the interference is 0.03 mm and the friction coefficient is 0.4, there is a minimum displacement of 1.36 mm, and when interference is 0.02 mm and the friction coefficient is 0.2, there is a maximum displacement of 3.25 mm. This indicates that the displacement of the CFRP core slightly decreases with increasing friction coefficient and interference.

To prevent radial pressure failure, the radial stress of the CFRP core must be less than the compressive strength of the CFRP core of 100 MPa, so the interference should be less than 0.025 mm.

D. VERIFICATION OF THE SIMULATION RESULTS

To validate the FEA results, a radial pressure test is carried out for the CFRP core. Test specimens are cut to lengths of 250 mm from production composite rods with a 6 mm diameter. Four identical samples are analyzed in individual radial pressure tests. Radial pressure testing of the prepared test samples is conducted using a 300 kN universal testing machine (UTM); this is illustrated in Figure 9(a).

The principle of the radial pressure test of the CFRP core is shown in Figure 9(b). The diameter of the plates used in the test is 150 mm. During the test, the CFRP core specimen is placed horizontally on the bottom plate and kept in the center with the plate. The top plate is pressed continuously at a loading rate of 1 mm/min until the core fails. Then, the testing machine is unloaded, and the deformation data are measured. The CFRP core test samples before and after the test are represented in Figure 10.

In the measurement of the diameter of the CFRP core after radial pressure failure, a micrometer with an accuracy of 0.002 mm is used to take the average value of readings at two different positions in the compressive failure zone.

To validate the FEA results, two sets of simulation results are taken and compared with tests. In the first case, the interference is 0.025 mm, the angle is 2°, and the friction coefficient is 0.2. In the second case, the interference is 0.0275 mm, the angle is 3°, and the friction coefficient is 0.3. The radial deformation of the CFRP core in these two cases is shown in Figure 11.

The difference between the diameter before and after the test of the CFRP core is the deformation value of the core. A comparison of the experimentally and numerically obtained radial deformation values for the CFRP core after radial pressure failure is tabularized in Table 4. Because the CFRP core is deformed on both the top and bottom, the total deformation of the CFRP core is twice the maximum deformation.

Within the margin of error, the table shows that the deformation values of the experimental results exhibit good

agreement with the numerical results, which confirms the analysis results. The numerical radial deformation are have slightly higher values than the experimental results, which can be primarily attributed to the simplifications in the modeling of the CFRP core, i.e., neglecting carbon fibers and glass fibers and thermal action.

VI. CONCLUSION

This study was carried out to investigate the failure modes of CFRP cores with self-tightening strain clamps. For that goal, FEA was conducted on the parameters affecting the radial stress and displacement of the CFRP core. The analysis results revealed that the radial stress of the CFRP core decreased with lower interference. However, this also resulted in the loss of the radial clamping force generated by the interference and wedge reaction force, leading to the lack of confining force necessary for self-tightening and subsequently to the occurrence of slip failure. In the case of interference of 0.025 mm, it appeared that the radial stress reached the radial compressive strength of the CFRP core of 100 MPa. In the case of interference lower than 0.02 mm, an angle lower than 1°, and a friction coefficient lower than 0.2, slip failure occurred in the core. Based upon these results, the optimal parameters appeared to be an interference between 0.02 mm and 0.025 mm, an inner wedge with an angle larger than 3°, and a friction coefficient larger than 0.3. Finally, radial pressure tests were carried out to verify the analysis results. The experimental results showed that the sample yielded the same deformation values as the FEA results, which confirmed the analysis results.

This study holds promise for preventing the failure of CFRP cores with self-tightening strain clamps. Future work will consider the combined action of three factors, the interference, angle and friction coefficient, on the failure modes and consider the effects of more factors.

REFERENCES

[1] B. Noor, M. Z. Abbasi, S. S. Qureshi, and S. Ahmed, "Temperature and wind impacts on sag and tension of AAAC overhead transmission line," *Int. J. Adv. Appl. Sci.*, vol. 5, no. 2, pp. 14–18, Feb. 2018.

[2] M. A. Alaqil and K. Kopsidas, "Modeling multi-layer OHL conductors undergoing wind-induced motion," *IEEE Access*, vol. 8, pp. 104579–104589, 2020.

[3] M. Frigerio, P. B. Buehlmann, J. Buchheim, S. R. Holdsworth, S. Dinser, C. M. Franck, K. Papailiou, and E. Mazza, "Analysis of the tensile response of a stranded conductor using a 3D finite element model," *Int. J. Mech. Sci.*, vol. 106, pp. 176–183, Feb. 2016.

[4] G. S. Shivashankar and Poornima, "Overview of different overhead transmission line conductors," *Mater. Today, Proc.*, vol. 4, no. 10, pp. 11318–11324, 2017.

[5] D. W. Zhang, Q. Zhang, X. G. Fan, and S. D. Zhao, "Review on joining process of carbon fiber-reinforced polymer and metal: Applications and outlook," *Rare Metal Mat. Eng.*, vol. 48, pp. 44–54, Jan. 2019.

[6] S. Kumar, G. Pal, and T. Shah, "High performance overhead power lines with carbon nanostructures for transmission and distribution of electricity from renewable sources," *J. Cleaner Prod.*, vol. 145, pp. 180–187, Mar. 2017.

[7] M. Z. Abbasi, B. Noor, M. A. Aman, S. Farooqi, and F. W. Karam, "An investigation of temperature and wind impact on ACSR transmission line sag and tension," *Eng., Technol. Appl. Sci. Res.*, vol. 8, no. 3, pp. 3009–3012, Jun. 2018.

[8] B. Burks, D. Armentrout, and M. Kumosa, "Failure prediction analysis of an ACCC conductor subjected to thermal and mechanical stresses," *IEEE Trans. Dielectr. Electr. Insul.*, vol. 17, no. 2, pp. 588–596, Apr. 2010.

[9] E. Hakansson, P. Predecki, and M. S. Kumosa, "Galvanic corrosion of high temperature low sag aluminum conductor composite core and conventional aluminum conductor steel reinforced overhead high voltage conductors," *IEEE Trans. Rel.*, vol. 64, no. 3, pp. 928–934, Sep. 2015.

[10] J. Geng, S. Zhou, and X. Qi, "Contrastive study on corona characteristics of aluminum conductor composite core and aluminum conductor steel reinforced," *Electr. Power*, vol. 48, pp. 76–80, Jan. 2015.

[11] Z. Cheng, "Thermal characteristics of aluminum conductor composite core," *J. Coast. Res.*, vol. 83, pp. 356–358, 2018.

[12] C. Liu, Y. Zhang, M. Shen, and X. Qi, "Sag characteristics of aluminum conductor composite core under high temperature conditions," *Water Res. Power*, vol. 31, pp. 210–212, Sep. 2013.

[13] G. Zhao, J. Wang, W. Hao, Y. Luo, and G. Guo, "Creep life evaluation of aluminum conductor composite core utilized in high voltage electric transmission," *Polym. Test.*, vol. 63, pp. 573–581, Oct. 2017.

[14] A. A. Alawar, E. J. Bosze, and S. Nutt, "High temperature strength and creep of an al composite with a hybrid composite core," in *Proc. Int. Conf. Compos. Mater.*, Kyoto, Japan, Jul. 2007, pp. 8–13.

[15] A. Alawar, E. J. Bosze, and S. R. Nutt, "A composite core conductor for low sag at high temperatures," *IEEE Trans. Power Del.*, vol. 20, no. 3, pp. 2193–2199, Jul. 2005.

[16] S. Du and B. Z. Zang, "Optimization of electric transmission line of power grid with carbon fiber composite core conductor," *J. Elect. Syst.*, vol. 15, no. 3, pp. 448–458, Sep. 2019.

[17] M. S, N. Srinivas, Y. S. Siddarth, C. V. S. Kamal, K. Sudheendra, S. Bhowmik, M. K. Pitchan, and J. A. Epaarachchi, "Numerical analysis of state of the art high performance thermoplastic composite as light weight bullet proof material," *Mater. Res. Exp.*, vol. 6, no. 9, Jul. 2019, Art. no. 095333.

[18] S. Margabandu and S. Subramaniam, "Experimental evaluation and numerical validation of bending and impact behaviours of hybrid composites with various stacking arrangements," *Mater. Res. Exp.*, vol. 6, no. 12, Nov. 2019, Art. no. 125305.

[19] R. M. Brunair, G. E. Ramey, and R. R. Duncan, "An experimental evaluation of S-N curves and validity of Miner's cumulative damage hypothesis for an ACSR conductor," *IEEE Trans. Power Del.*, vol. 3, no. 3, pp. 1131–1140, Jul. 1988.

[20] A. Cardou, L. Cloutier, J. Lanteigne, and P. M'Boup, "Fatigue strength characterization of ACSR electrical conductors at suspension clamps," *Electr. Power Syst. Res.*, vol. 19, no. 1, pp. 61–71, Jul. 1990.

[21] N. K. Kar, Y. Hu, E. Barjasteh, and S. R. Nutt, "Tension–tension fatigue of hybrid composite rods," *Compos. B, Eng.*, vol. 43, no. 5, pp. 2115–2124, Jul. 2012.

[22] J. S. Park, W. T. Jung, J. Y. Kang, and M. S. Kum, "Behavior characteristics of bonded type anchorage for CFRP tendon," *Engineering*, vol. 5, no. 11, pp. 909–918, 2013.

[23] H.-Y. Yu, L. Wang, R. Li, M.-B. Yu, M. Qian, Z.-X. Li, G.-Y. Li, Z.-H. Zhu, Q. Yuan, and X. Dong, "Analysis on the tensile failure modes of carbon fiber composite core rod used in overhead stranded wires," *Electr. Power*, vol. 47, pp. 49–52, 5 Jan. 2014.

[24] R. Wang, H. Zobeiri, H. Lin, W. Qu, X. Bai, C. Deng, and X. Wang, "Anisotropic thermal conductivities and structure in lignin-based microscale carbon fibers," *Carbon*, vol. 147, pp. 58–69, Jun. 2019.

[25] S. Chinkanjanarot, J. M. Tomasi, J. A. King, and G. M. Odegard, "Thermal conductivity of graphene nanoplatelet/cycloaliphatic epoxy composites: Multiscale modeling," *Carbon*, vol. 140, pp. 653–663, Dec. 2018.

[26] S. Ogihara and S. Moriwaki, "Tensile creep deformation in unidirectional carbon/epoxy laminates under off-axis loading," *J. Mater. Sci.*, vol. 39, no. 10, pp. 3465–3467, May 2004.

[27] M. Tane, H. Okuda, and F. Tanaka, "Nanocomposite microstructures dominating anisotropic elastic modulus in carbon fibers," *Acta Mater.*, vol. 166, pp. 75–84, Mar. 2019.

[28] Y. Yan and Y. Duan, "A finite element method of modelling and designing of an ACCC conductor," in *Proc. MATEC Web Conf.*, vol. 153, 2018, p. 01005.

[29] E. Stanova, G. Fedorko, S. Kmet, V. Molnar, and M. Fabian, "Finite element analysis of spiral strands with different shapes subjected to axial loads," *Adv. Eng. Softw.*, vol. 83, pp. 45–58, May 2015.

[30] S. Kmet, E. Stanova, G. Fedorko, M. Fabian, and J. Brodniansky, "Experimental investigation and finite element analysis of a four-layered spiral strand bent over a curved support," *Eng. Struct.*, vol. 57, pp. 475–483, Dec. 2013.

[31] G. Fedorko, E. Stanova, V. Molnar, N. Husakova, and S. Kmet, "Computer modelling and finite element analysis of spiral triangular strands," *Adv. Eng. Softw.*, vol. 73, pp. 11–21, Jul. 2014.

[32] M. H. Yu, "Advances in strength theories for materials under complex stress state in the 20th century," *Adv. Mech.*, vol. 34, pp. 529–560, May 2004.

HONGBO CHEN received the B.S. degree from Xi'an Jiaotong University, China, in 1996, and the M.S. degree from Wuhan University, China, in 2012.

Since 2000, he has been an Engineer with the State Grid Corporation of China, where he has been engaged in power line operation and maintenance. His research interests include electrical insulation and cables and electrical engineering.

JIAYUN CAO received the B.S. degree in materials science and engineering from the Chengdu University of Technology, China, in 2004. He is currently pursuing the M.S. degree with Sichuan University, China.

His research interest includes simulation analysis of failure of carbon fiber composite core.

XIAOMIN ZHANG received the B.S. and M.S. degrees in materials science and engineering from Sichuan University, China, in 2010 and 2013, respectively.

Since 2013, she has been an Engineer with the State Grid Corporation of China, where she has been engaged in material testing. Her research interest includes testing and analysis of mechanical properties of materials.

YU JIANG received the B.S. degree in materials science and engineering from the Chengdu University of Science and Technology, China, in 1993, and the M.S. and Ph.D. degrees in materials science and engineering from Sichuan University, China, in 1996 and 2004, respectively.

His research interests include computational materials science and analysis of materials failure.

• • •